Bulletin of Geophysics and Oceanography Vol. 62, n. 3, pp. 365-386; September 2021
DOI 10.4430/bgo00361

Chirp data processing for fluid flow detection at the Gulf of Trieste (northern Adriatic Sea)

A. Vesnaver, M. Busetti and L. Baradello

Istituto Nazionale di Oceanografia e di Geofisica Sperimentale - OGS, Trieste, Italy

(Received: 23 January 2021; accepted: 7 May 2021; published online: 20 September 2021)

ABSTRACT Recent studies revealed the emission of fluids from the seafloor at various locations in the Gulf of Trieste (northern Adriatic Sea). To image the shallow sediments where this happens, several Chirp surveys were carried out. The shallow water reverberations limited the interpretation of this data, so we set up a workflow that attenuated the multiple reflections significantly. The new images of the shallow formations allowed improving our understanding of the most recent geological phenomena. Also, faint reflections from water layers with different acoustic impedance, probably due to temperature differences, were revealed, and several plumes were imaged. These images allow linking the shallow stratigraphy of the seafloor to ongoing fluids' emissions.

Key words: Chirp, dereverberation, fluid emission, multiple reflections, Gulf of Trieste.

1. Introduction

The Chirp technology has been developed originally for military, fishery, and engineering applications (Kim *et al*., 1999; Ehrenberg and Torkelson, 2000), whose main target is delineating precisely the seafloor and estimating its hardness. Geophysical applications extended this initial goal to imaging the shallow sediments below the seafloor. Indeed, Chirp surveys are very effective in filling a frequency range, where other geophysical methods struggle, i.e. between a few hundred and several thousand Hz. The signal emitted by the source is controlled and can be correlated with the reflected signals backscattered by the subsurface geological interfaces. Doing so, we convert the waveform (or sweep) emitted by the source into a zero-phase Klauder wavelet (see e.g. Baeten and Ziolkowski, 1990). Chirp data are converted usually to complex traces by a Hilbert transform and only their envelope is retained, as the resulting image allows an easier interpretation (Henkart, 2006). If data are recorded in the original correlated waveform, a few processing tools can be used as for seismic data, i.e. predictive and FX deconvolution (Baradello, 2014), which improve the Earth imaging even better.

Correlated data are rarely provided directly from the acquisition system, as in the case of the pioneering applications presented by Quinn *et al.* (1998), and so the more accurate processing tools mentioned above become inappropriate. In this case, the removal of shallow water reverberations by advanced techniques based on the wave equation, as the seafloor multiple modelling and elimination (Wiggins, 1988; Verschuur *et al.,* 1992; Pham and Lau, 1997, among others) becomes a border-line option, as the phase behaviour of the signal is missing. Even better options require a multi-channel recording system, as the FK-domain multiple elimination based on the different move-out between multiples and primaries (Cassano and Rocca, 1973; Taner, 1980; Yilmaz, 2001) or using the Radon transform (Kelamis and Mitchell, 1989; Foster and Mosher, 1992).

Chirp data are single channel records, where the source and receiver locations are coincident, as for the theoretical zero-offset traces in seismic surveys. Because of this recording limitation, we must simplify our Earth model by a local 1D approximation. We cannot detect the precise signal direction, indeed, so we can only expect a near-vertical propagation direction for reflections where the seafloor and the shallowest layers are horizontal and almost flat. This is the case for the field experiment analysed in this paper. The workflow presented here is based on this assumption, and it breaks down for cases with a rugged and dipping bathymetry. We are comparing this approach with conventional deconvolution techniques, to highlight shallow anomalies and even possible fluid plumes in the Gulf of Trieste (northern Adriatic Sea).

The presence of fluids is well documented in the Adriatic Sea (Conti *et al.,* 2002). Hydrocarbon exploration highlighted that the Plio-Quaternary terrigenous sediments contain biogenic gas (e.g. Casero, 2004). In the Gulf of Trieste, these units drape the bedrock constituted by the Eocene to Miocene Gallare Marls and the Miocene Cavanella formation on the west and the Eocene turbidites in the central-eastern part, with a few hundred metre of thickness in the western part and pinching out eastwards (Busetti *et al*., 2010; Vesnaver *et al*., 2020).

Multichannel seismic data acquired in the Gulf of Trieste show evidence of fluid occurrence and migration within the Plio-Quaternary sediment by very low amplitude signals, within areas that may reach an extension of several hundred metres when observed along the seismic profile (Busetti *et al*., 2013). Gas pockets in the shallow Late Pleistocene deposit are well imaged by Chirp data (Gordini *et al*., 2004, 2012; Busetti *et al*., 2020). The acoustic evidence of the fluid is the high-amplitude reflector overlying blanking zones, where the acoustic signal is almost absent. This blanking is caused by the strong attenuation of the high frequencies due to anelastic absorption and scattering by gas bubbles within the sediments. As a consequence, only the top of the gas bearing horizon provides a reflection, while the underlying sediments are "transparent" (Tóth *et al*., 2014).

Occasionally, fluids may seep into the water column, where the gas pockets are very close to the seafloor. The gas seeping could reach the sea surface producing a gurgle effect. This phenomenon is well known by the local population, which call it "bromboli", and was documented for the first time by Morgante (1940).

On the seabed, associated with gas emissions, there are frequently rocky outcrops made up of cemented sands often covered by organogenic concretions. The origin of these outcrops may be due to the precipitation of methane-derived calcium carbonate cementing the unconsolidated sediments. They are colonised by organisms, some of which are bio-constructors (Gordini *et al*., 2012). In the northern Adriatic Sea, these outcrops, known as "trezze", are very frequent, and about 250 have been identified in the Gulf of Trieste (Gordini *et al*., 2003, 2004). Chemical analyses by Gordini *et al.* (2012) revealed that gas consists primarily of methane (81-84%), nitrogen (15-18%) and oxygen (0.7-1.3%), and radiocarbon ^{14}C datation reveals that the methane dates back to Late Pleistocene, rising from organic rich peat layers, but contribution from deeper and older layers are not excluded (see also Hovland and Curzi, 1989; Busetti *et al.*, 2013).

Chirp data highlight the presence of gas plumes in the water column. However, this acoustic signal is ambiguous sometimes, as acoustic vertical noises may be present too. The aim of this paper is trying to distinguish between the acoustic evidence of the plume and the noise, to provide a consistent interpretation of the gas seeping within the water column and to improve the imaging of fluid occurrence within the sediments.

2. Chirp data processing

We processed part of the lines G05-C02 and GT09-C21, acquired by OGS (National Institute of Oceanography and Applied Geophysics) in the Gulf of Trieste (north-eastern Adriatic Sea) in 2005 and 2009, respectively (Fig. 1). The GT09-C21 profile images several fluid accumulations within the shallow sediments as well as fluid plumes in the water column (Fig. 2).

The Chirp acquisition system is a Benthos CAP-6600 Chirp II Data-Sonics, with a source and 16 receivers hull-mounted on board of R/V OGS Explora at 4.32 m depth, with a frequency range sweeping from 2 to 7 kHz, a sampling interval of 0.066 ms and shooting frequency of 12 times per second. During the processing, a resampling to 0.2 ms was carried out to reduce the data size, so ending up to a Nyquist frequency of 2500 Hz, which is sufficient for our purposes. The Chirp data was recorded in reflectivity mode. The seafloor depth ranges from 12.9 to 15.5 m along the profile G09-C02 and from 13.6 to 25.0 m along the profile GT09-C21, considering an average sea water velocity in the study area of 1514 m/s (Trobec *et al*., 2018).

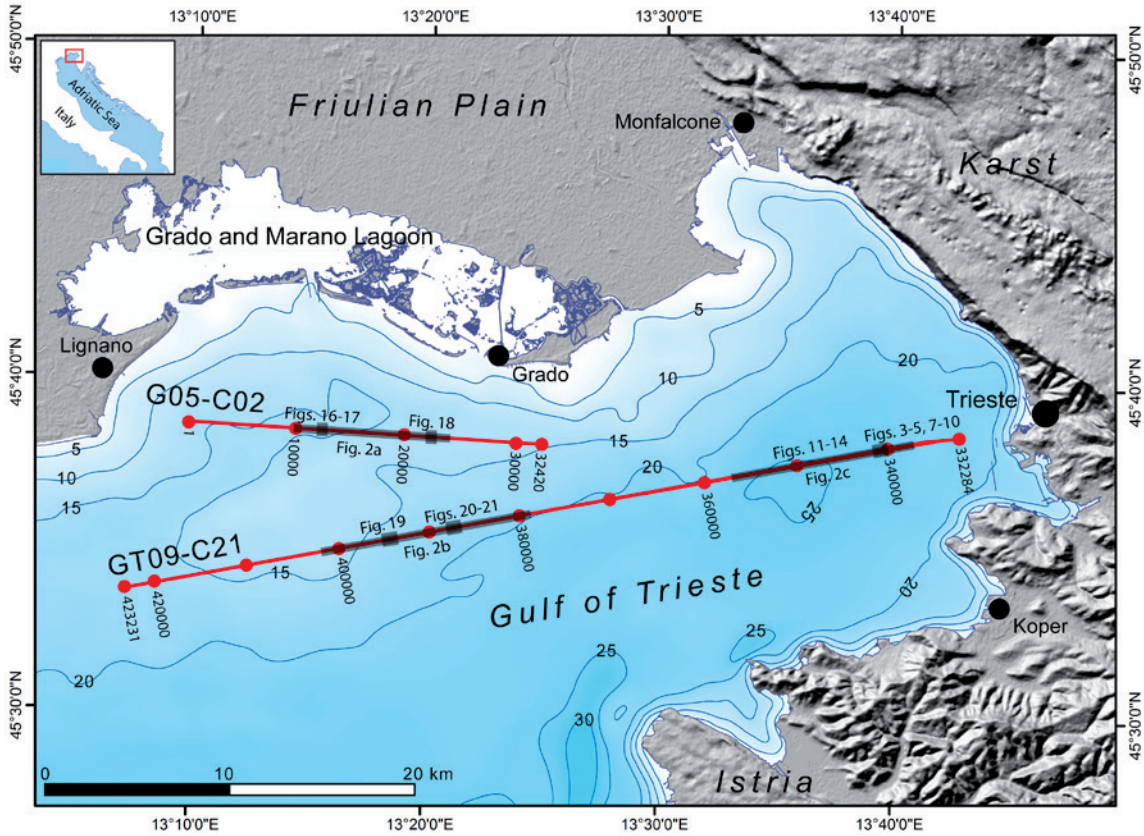

Fig. 1 - The Gulf of Trieste (northern Adriatic Sea) with the location of the Chirp profiles G05-02 and GT09-C21 acquired in 2005 and 2009, respectively, by the R/V OGS Explora. Annotations along the profiles indicate the shot point number. Bathymetric contours are expressed in metres. The bathymetric model is obtained from Zampa (2020), merging data from EMODnet Bathymetry Consortium (2018) and Trobec *et al.* (2018).

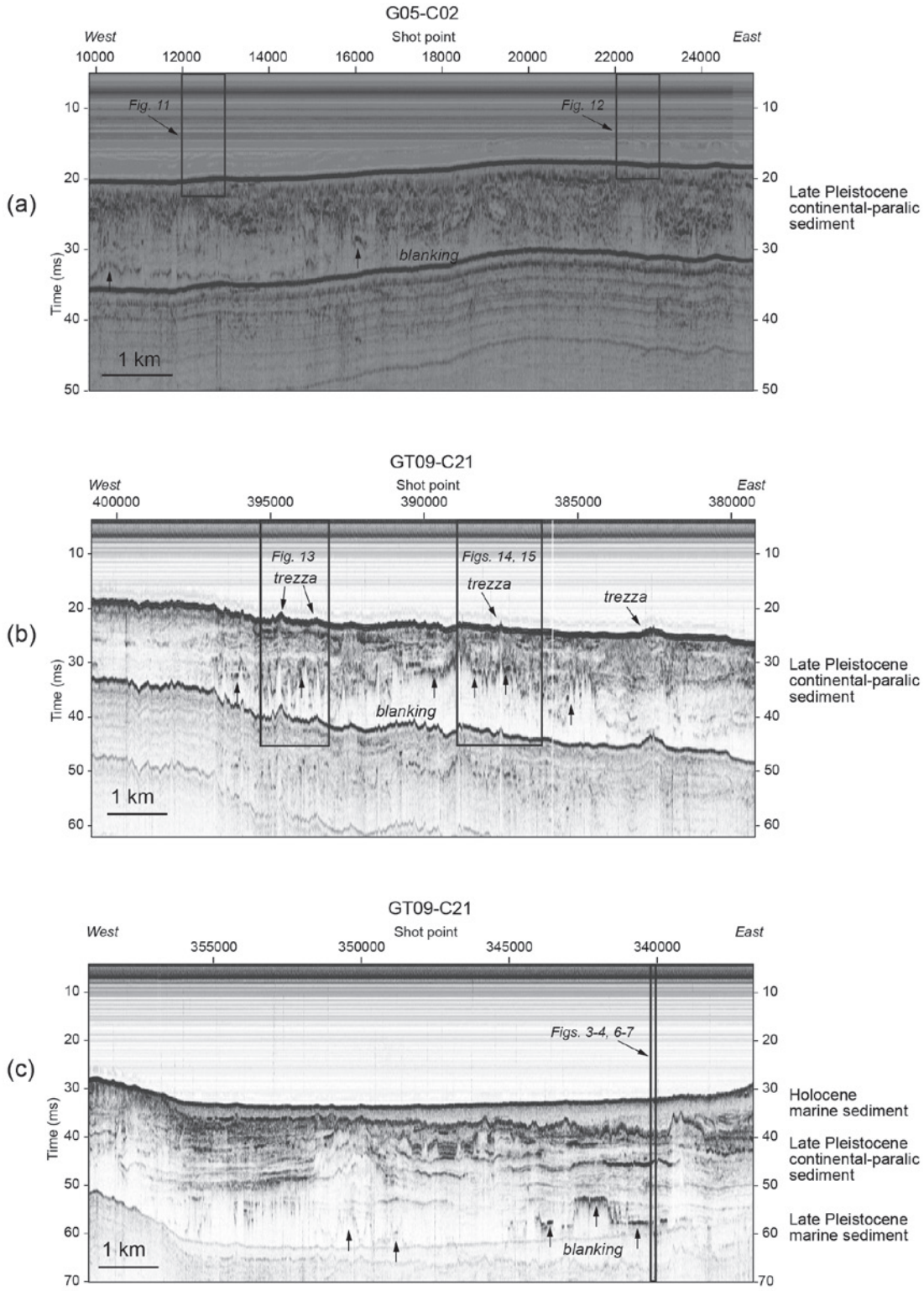

Fig. 2 - Raw data of the Chirp profiles G05-C02 (a) and GT09-C21 (b and c), whose location is presented in Fig. 1. The black arrows indicate the enhanced amplitude reflectors at the top of the blanked zones, related to fluid bearing sediments. Boxes and arrows indicate the profiles' parts that have been expanded and analised further in the rest of the paper

2.1. Gain curve

Fig. 3 displays a sample of GT09-C21 raw data, i.e. 120 traces with a common normalising factor to optimise the signal image. We see two prominent signals: the seafloor reflection at about 30 ms, and the first arrival at 1-4 ms. The latter one corresponds to the signal scattered from a nearby object to the receiver. The 16 sensors that form the Chirp system are embedded in a box containing distilled water with a titanium wall that separates them from the seawater. This interface generates the first recorded reflected signal. Fig. 3 allows comparing different algorithms for compensating the amplitude decay of signals due to the geometrical spreading and anelastic absorption. A simple normalisation trace-by-trace (Fig. 3b) introduces strong artefacts as vertical bars, while does not enhance any deep reflection. Applying an Automatic Gain Control (AGC) with a time window of 15 ms (Fig. 3c), the initial spurious arrivals are attenuated a bit better, as well as the vertical bars, which are still present. However, AGC distorts some information that we are seeking, i.e. possible reflectivity variations along and below the seafloor. On the positive side, AGC highlights primary reflections between the seafloor (at about 29 ms) and its first multiple (at about 58 ms), suggesting that we might get further signals, if that multiple could be removed.

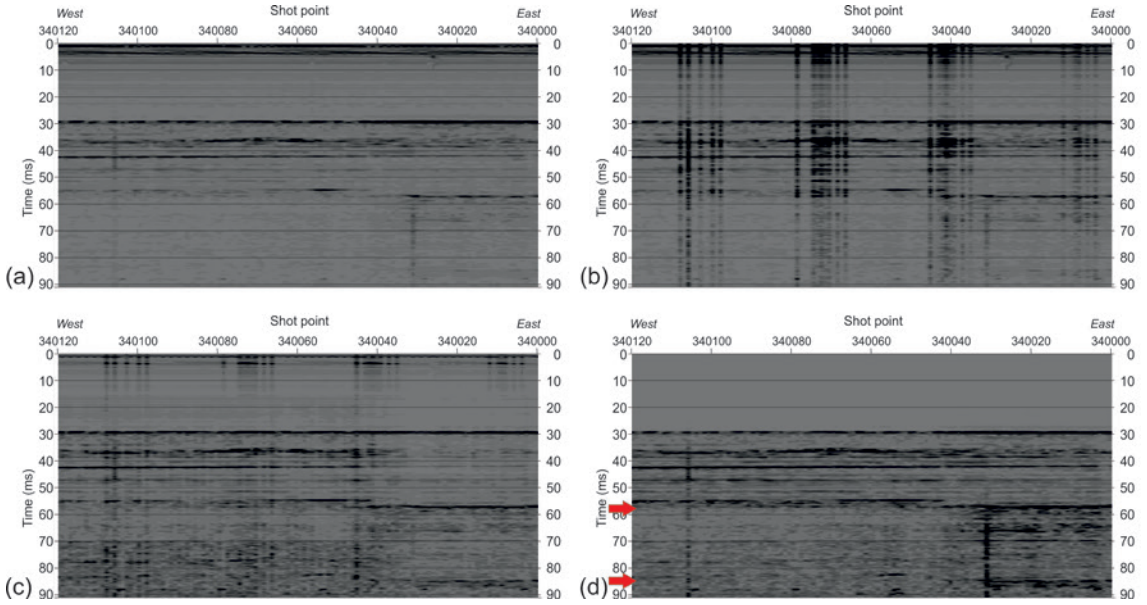

Fig. 3 - The GT09-C21 data sub-set used for the processing parameter choice, after a global scaling factor for the display optimisation (a), after a normalisation on a trace-by-trace basis (b), by an AGC, using a time window of 15 ms (b) and after a normalisation by a t^2 gain curve (d). The red arrows point to the start of the first and second multiples' train.

To avoid the dominance of the first arrival and the seafloor reflection when applying a normalisation, we multiplied each trace sample by the square of its arrival time (Fig. 3d), as suggested by Fowler and Claerbout (1983). In their paper, they show that a simple power of 1 for the time parameter can account for the spherical divergence, while a power of 2 includes an approximated compensation for the anelastic absorption. Of course, this is just a rule of thumb; however, this compensation reduces the contribution of shallow events, greatly reinforcing the deeper ones. We cannot compensate more accurately the amplitude decay by allowing for the vertical velocity layering, as we cannot estimate seismic velocity from single-

channel records. Although this gain curve is heuristic, its application does not modify heavily the relative amplitudes of shallow events, as the AGC does, so preserving better the seismic stratigraphy. Doing so, the vertical bands almost disappeared, and deeper events showed up better between the seafloor and its first multiple reflection. There are lateral variations of reflectivity along the seafloor (at 29 ms) that are not correlated with the scattered signals from the sea surface (between 1 and 4 ms).

2.2. Multiple attenuation by gapped deconvolution

The removal of the seafloor multiples is our next challenge. A gapped deconvolution has been the horse-work for decades for single-channel seismic processing [see e.g. Yilmaz (2001), among many others]. It is a stochastic processing, i.e. not based on the wave equation. It assumes that a trace is the convolution of a minimum-phase wavelet with a series of reflection coefficients that is white, i.e. with a constant amplitude spectrum. The deconvolution operator is designed by inspecting the traces autocorrelation and the t^2-equalised data. The seafloor is located at about 29 ms in the time section (Fig. 3c), while the autocorrelation is populated significantly up to the multiple lag (about 28 ms). Thus, we chose a Wiener prediction error filter or, in jargon, gapped deconvolution, with an operator whose terms range from 25 to 50 ms. The deconvolution (Fig. 4a) shows that both the first (at 58 ms) and the second seafloor multiple (at 85 ms) were significantly attenuated.

There are mathematical reasons to explain this processing success. In the predictive deconvolution theory (Robinson, 1967, 1983), a seismic trace $s(t)$ is modelled by the convolution of a seismic wavelet $w(t)$ with a reflectivity sequence $r(t)$:

$$s(t) = r(t) * w(t). \quad (1)$$

Taking the Hilbert transform H{.} of both equation sides and exploiting its properties, we get:

$$H\{s(t)\} = H\{r(t) * w(t)\} = r(t) * H\{w(t)\}. \quad (2)$$

Thus, the Hilbert transform of a trace is the convolution of reflectivity with the Hilbert transform of the wavelet, if (and only if) the trace can be approximated by a convolutory Earth model. Assuming the predictive deconvolution hypotheses, i.e. if the energy spectrum of the reflectivity is white (or constant), the autocorrelation of the trace $s(t)$ is proportional to the energy spectrum of the Hilbert-transformed wavelet H{$w(t)$}. The next hypothesis, however, is particularly tight: we can retrieve a wavelet from its autocorrelation unambiguously if (and only if) such a wavelet is minimum phase (Robinson and Treitel, 1980). This ideal condition is never met in real experiments, but impulsive sources approximate fairly this hypothesis, and the consequent processing results are often satisfying. Having these limitations in mind, we can use a gapped deconvolution for the multiples' attenuation, while expecting some moderate distortion of the seismic signals (see the Appendix for further details).

2.3. Multiple attenuation by subtraction

An alternative strategy for multiple attenuation in seismic data is their modelling and subtraction. However, the Chirp data cannot be predicted directly by the wave equation, as presented by

Wigging (1988), both for the enveloped waveforms and the single-channel acquisition. However, if the reflectivity below the seafloor is weak, we may assume as primaries all the reflections arriving between t_{WB} and 2 t_{WB}, where t_{WB} is the two-way traveltime between the source and the water bottom. This is accurate if the source depth is much smaller than the seafloor depth, otherwise some correction is needed.

We picked the seafloor by a semi-automatic algorithm. We picked manually t_{WB} in the first record of the survey and extracted the waveform related to the seafloor reflection. The current time was chosen as the centre for a window search in the following trace, cross-correlating the reference wavelet with the current trace. The time where this correlation is maximum is picked as the t_{WB} for the current trace, becoming the starting point for a search in the next one, and so on in a sequence. As the seafloor is almost flat, without abrupt signal discontinuities, the procedure worked nicely.

Fig. 4b is the result of subtracting the first multiples' train from the data in Fig. 3d, i.e. after the amplitude recovery by the t^2 curve. The result is not so different than what we obtained by the gapped deconvolution (Fig. 4a) when it comes to the first multiple removal, between 55 and 65 ms, while only the gapped deconvolution can reduce also the second multiple train at about 85 ms, despite its weakness. The green arrows show where the multiples were attenuated, while the red ones show where they are present.

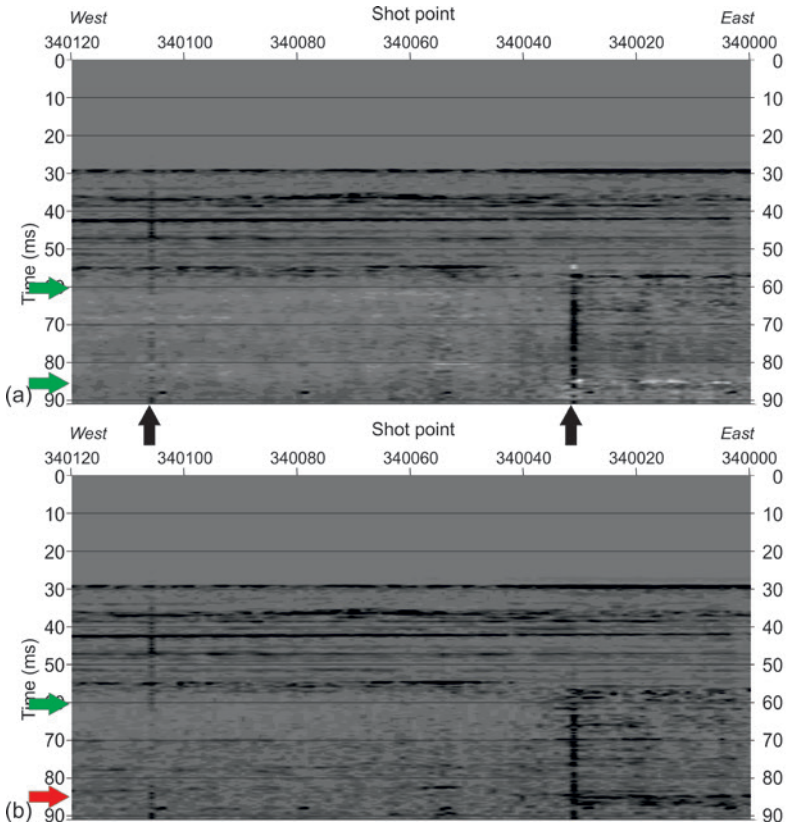

Fig. 4 - The GT09-C21 data in Fig. 3a, after a normalisation by a t^2 gain curve and a gapped deconvolution (a) and after a normalisation by a t^2 gain curve and the multiple subtraction (b). The black arrows highlight two "vertical bars" that remain in the section after these processing steps. The green arrows show the areas where multiples were attenuated. The red arrow highlights the unchanged area in panel b affected by the second multiples' train, which was not subtracted.

Fig. 5 shows the multiple subtraction steps for a trace of this survey. The first reflection from the seafloor is picked, getting the two-way traveltime t_w. This value is used to extract a time window from t_w to a bit less than 2 t_w. This portion of trace cannot be affected by long-period multiples, and certainly is backscattered by the sea surface, scaled by a reflection coefficient that approximates one. In Fig. 5a, this trace chunk is plotted by a red dotted line, after a shift applied to distinguish it from the trace, plotted in a continuous blue line. This primaries' train is, then, shifted to fit the first multiple peak by a cross-correlation, and, then, a scaling factor is applied to it, by imposing that the energy of the trace obtained by subtracting the primaries' train is minimum (Fig. 5b). There are two reasons for such a scaling factor. First, the t^2 gain recovery we applied works better for layered structures where anelastic absorption occurs, while the multiples' propagation in water attenuates quite less: we may have so a diverging correction between primaries and multiples. Second, the reflection coefficient of the seafloor is variable, and so the related multiples' energy is variable too. After the subtraction (Fig. 5c, red

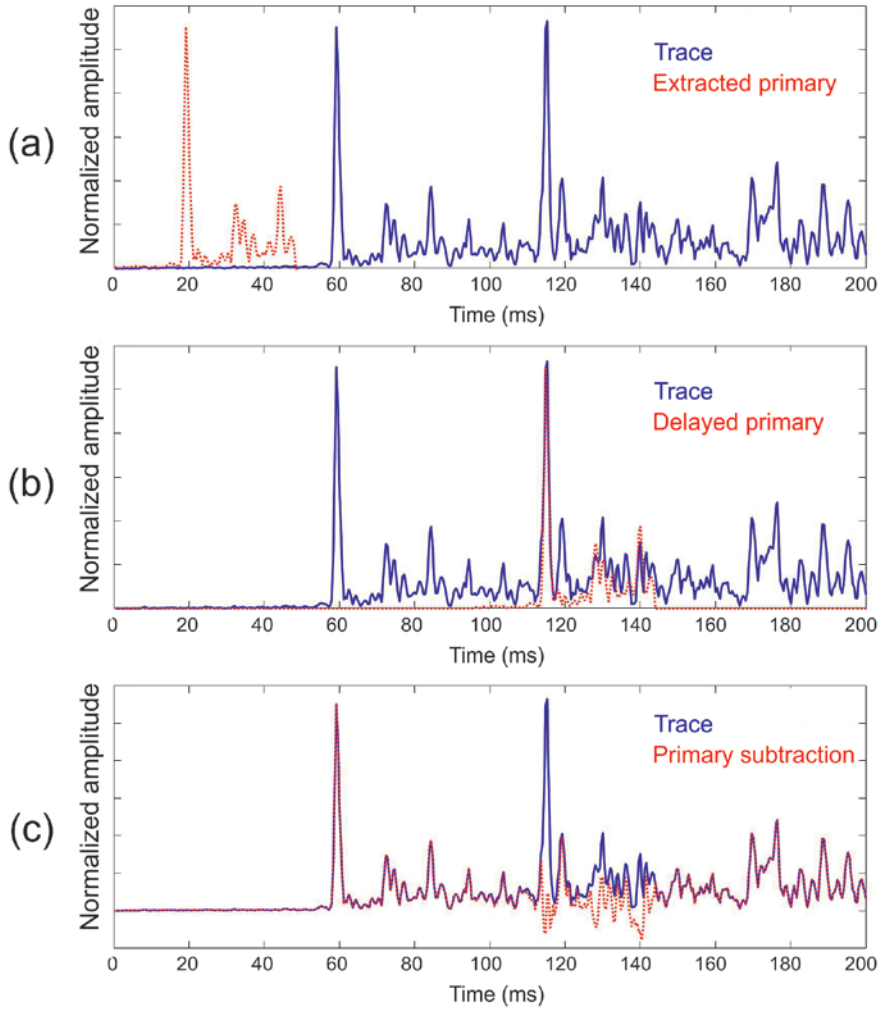

Fig. 5 - Key steps for the multiple subtraction procedure: primary part definition (a), alignment between primary part and first multiple (b), and subtraction by minimising the output energy (c). The continuous blue line shows always the input trace, while the red dotted line shows, in sequence, the extracted primary, its delayed version, and the subtraction result.

dotted line), the resulting trace looks “cleaner”, and we may expect to detect events that were otherwise overwhelmed by the multiples’ energy. Unfortunately, we get also a drawback, i.e. occasional negative values that are meaningless for an envelope, as a Chirp trace is. As an option, this negative part may be set to zero.

Fig. 6 allows comparing the effectiveness of multiple removal by the autocorrelation of the traces after the gain recovery (Fig. 6a), after the gapped deconvolution (Fig.6b) and after the multiple subtraction (Fig. 6c). For these plots, we used the same global equalisation factor, so that we can appreciate visually the amplitude decrease, which is stronger for the gapped deconvolution. To quantify this immediate feeling, we computed the average of the absolute value of the autocorrelations, getting values of 0.0023 for the input data, 0.0013 for the gapped deconvolution and 0.0022 for the multiple subtraction. Thus, the gapped deconvolution is clearly superior for the multiples’ removal from a numerical point of view. However, when looking at the resulting sections and trying to interpret them from a geological point of view, a different conclusion is probably preferable.

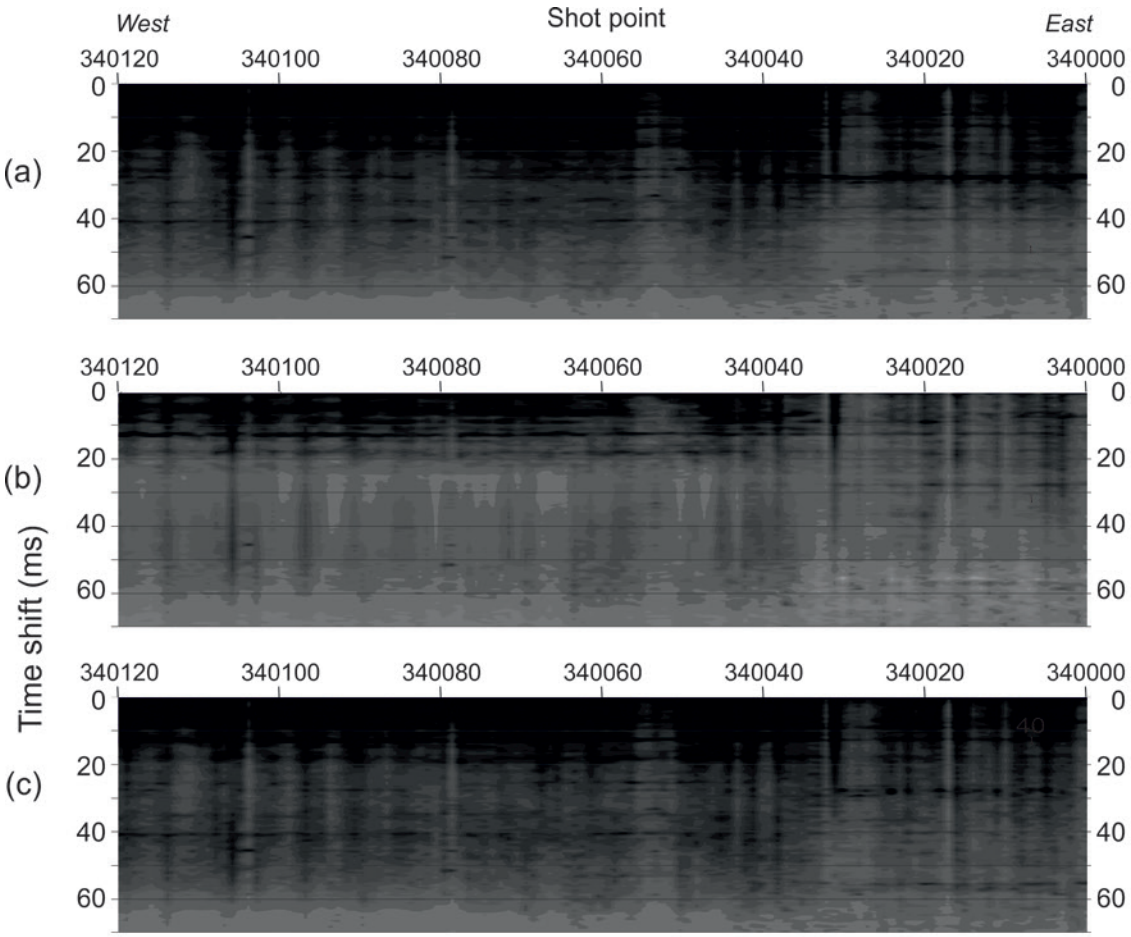

Fig. 6 - Autocorrelation of the GT09-C21 data: a) after the t^2 gain curve (Fig. 3d); b) after the gapped deconvolution (Fig. 4a) and c) after the multiple subtraction (Fig. 4b).

2.4. FX deconvolution

After attenuating a spatially organised noise as the multiples, the next step is reducing the random noise. FX deconvolution (Canales, 1984; Gulunay, 1986, 2017) is a classical tool for this goal. After converting each trace from time to frequency domain, it uses a complex Wiener filter for a given frequency, along the *x* coordinate along the profile, to separate the laterally coherent signal from the incoherent random noise. This technique relies on the general assumptions that geologically meaningful variations are smooth and continue, while features detected in just one or at most two adjacent traces only are spurious. This assumption is often true, but sharp and very local anomalies occur in nature too, and so we must be careful when interpreting seismic sections where such a filtering has been applied.

The comparison between Figs. 4a and 7 gives us an immediate flavour of the pros and cons for the FX deconvolution. The main advantage is the random noise reduction, while a disadvantage is the smearing of stronger continuous events, which may overwhelm the shorter, scattered ones. The only difference between the last two figures is the size of the Wiener filter: a relatively common choice of 30 traces (Fig. 7a) and the minimum possible size of 3 traces (Fig. 7b). The latter one is quite noisier than the other with a much longer window, but it preserves much better some local variations of reflectivity along the main horizons. Also, it removes nicely the two remaining vertical

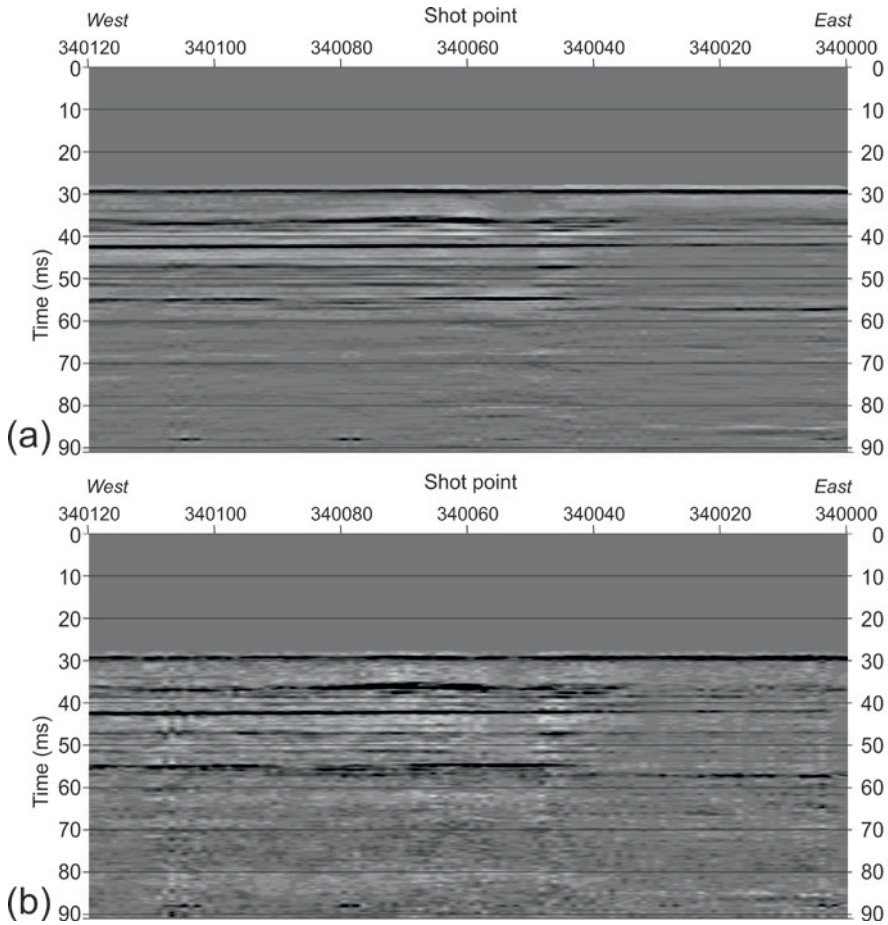

Fig. 7 - The Chirp profile GT09-C21 after a t^2 gain curve, a gapped deconvolution and a final normalisation with FX deconvolution using a lateral window of 30 traces (a) and 3 traces only (b).

bars still present in Fig. 6. The longer window (Fig. 7a) is definitely good looking, and still we can appreciate there some smooth reflectivity changes. On the other hand, some minor local features have been smeared out. Choosing between these two extreme options is a matter of personal preferences, as both get and loose some information.

Based on the results obtained for the data subset of 120 traces considered so far, we applied the same processing sequence to 15,000 traces of the profile. Fig. 8a displays part of the Chirp section after a t^2 gain recovery. Below the seafloor at 30 ms, several reflectors show up between 30 and 40 ms, characterised by rugged and discontinuous horizons. The very shallow Holocene sediments, just below the seafloor, are almost blank for a time span of 5 ms on the right and thins to 2 ms on the left side. The bottom of this formation is a continuous, but irregular strong reflector, corresponding to the continental/brackish surface prior to the Holocene marine transgression. It overlies other strong and irregular events, mainly fluvial (channel levee systems) continental deposit. Between 40 and 60 ms, the reflectivity is much weaker, except for a prominent event between 50 and 55 ms on the right side, an enhanced reflection maybe associated with gassy sediments (Duarte *et al*., 2007). From 60 ms on, the section is dominated by the multiples of the seafloor and the underlying reflectors just mentioned. The black arrows indicate just a few major multiples, which are present but less visible in the whole section.

The gapped deconvolution (Fig. 8b) is very effective in removing the multiples of any order.

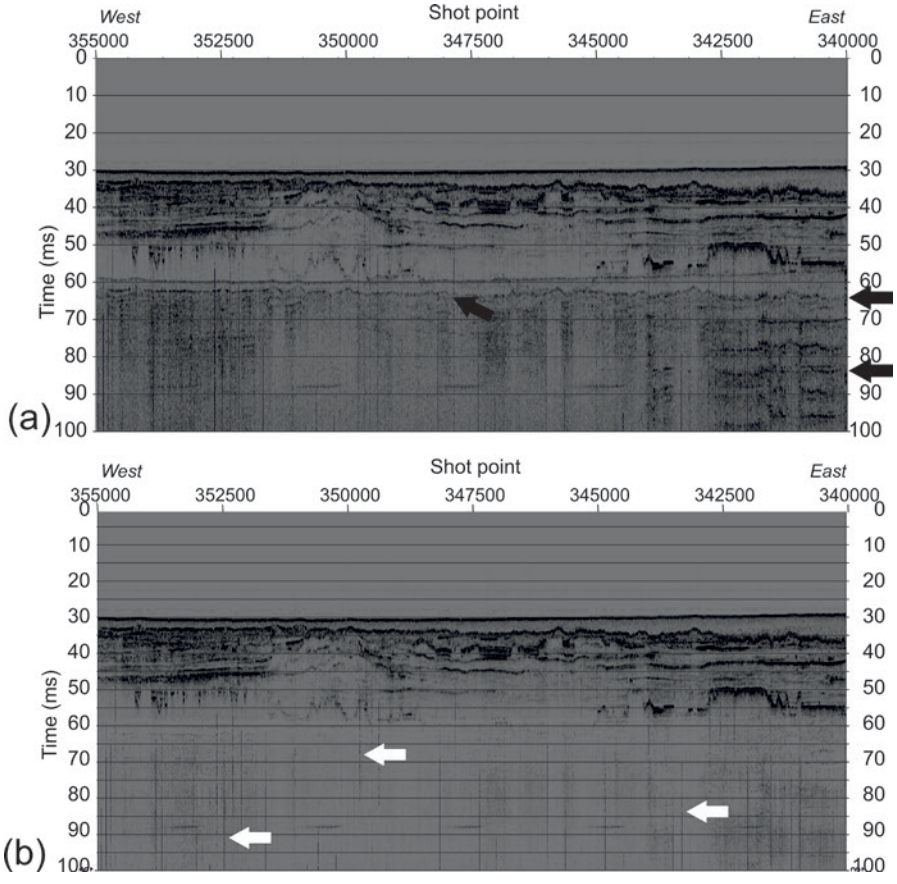

Fig. 8 - The Chirp profile GT09-C21 with after a normalisation by a t^2 gain only (a), followed by a gapped deconvolution (b). The black arrows point to a few more prominent multiples, while the white arrows show a few "vertical bars". The deconvolution removed the multiples very well, but possible underlying events are not evident.

Only a few very faint events can be seen in the central part, between 60 and 65 ms, which were previously already visible but overlapped to the multiples. A similar result is obtained by the first multiple subtraction (Fig. 9a), which is perhaps revealing a few more faint features between 60 and 65 ms, but obviously fails in removing the higher order multiples. Due to the weakness of the deeper reflectors and the limited penetration of the Chirp source, we do not expect to get further interpretable events by extending the multiple subtraction to higher orders. Throughout the section are visible "vertical bars" (which we discuss later), indicated by white arrows. They are more evident in the deeper part, where the reflected signals are weaker, and are missing above the seafloor, because the t^2 gain curve applied is strongly reducing their relative amplitude.

Applying the FX deconvolution to the data after the multiple subtraction (Fig. 9a), we get a cleaner image (Fig. 9b), where the lateral continuity of the broken events between 35 and 55 ms is enhanced. In the deeper part, below 60 ms, the background random noise is attenuated very much, whilst there are residuals of the "vertical bars" that are visible in Fig. 8b too. As the operator length for the FX deconvolution is 3 (traces), this means that those bars are not isolated disturbs, but local phenomena that are spatially organised.

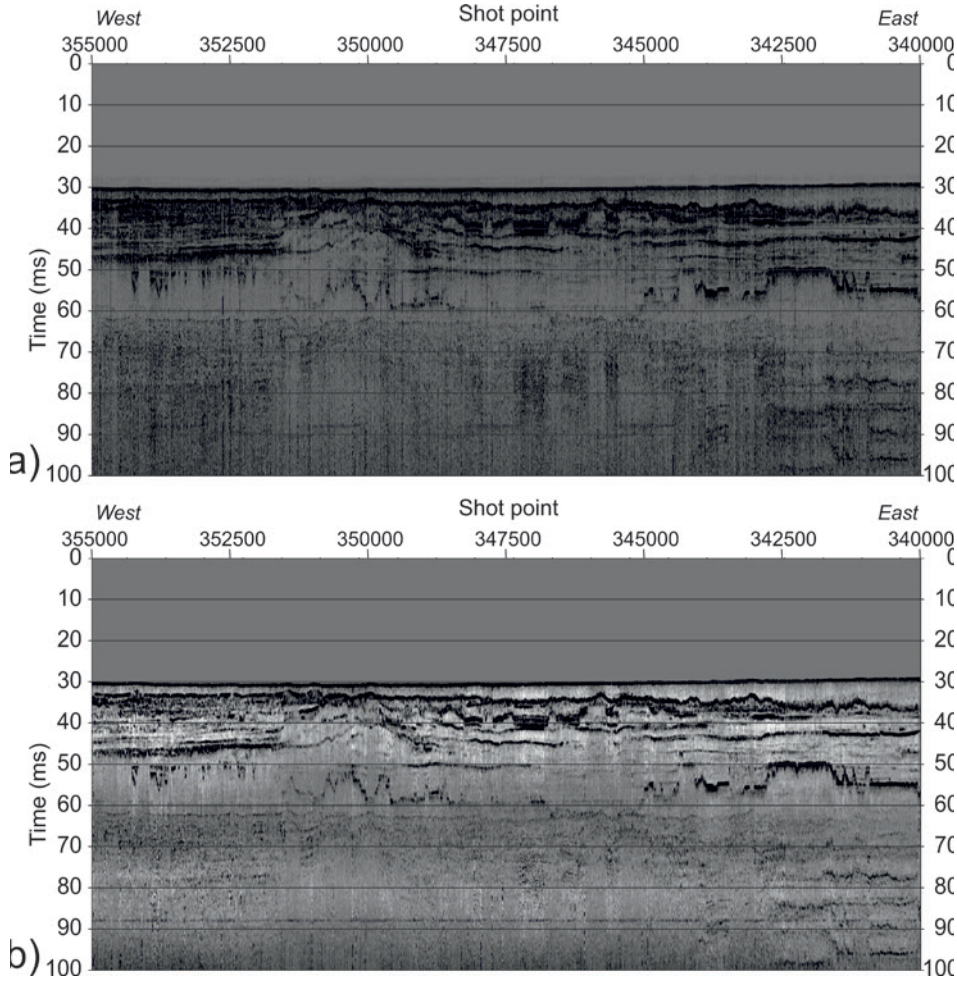

Fig. 9 - The Chirp profile GT09-C21 after the multiple subtraction (a), followed by a FX deconvolution with a lateral window of 3 traces only (b). In the lower figure, the random noise is significantly reduced and the sub-horizontal events are strengthened.

3. Sea water phenomena

Fig. 8b highlights well the shape of these bars, which are not affecting the traces at all arrival times, but only for a duration of 20 to 25 ms. Their shape is thin at the extrema and a bit wider in the central part. Their location in space and time is quite irregular. Two other examples of these vertical events are visible in Fig. 3d too: one from 30 to 50 ms around the shot point 340110, and another one from 60 to 85 ms around the shot point 340030. A possible explanation for these features is plumes of fluids emitted at the seafloor, acting intermittently as for geysers (Fig. 10). While moving from left to right, the acoustic wavefront emitted by source impinges first laterally, then centrally and finally laterally again on its main radiation lobe, which is optimised along a narrow angle in the vertical direction. Of course, this assumption should be validated by independent measurements and geological information, and at present is only a work hypothesis.

While the plumes' effect is just an hypothesis (García-Gil *et al*., 2002), the presence of different water layers is clearly proven by Fig. 11, displaying the seafloor and the shallowest reflections along the line G05-C02, acquired closer to the coast. We vertically exaggerated the time span from 4 to 20 ms, i.e. between the sea surface and seafloor, and used a large global scaling factor. Fig. 11a shows the data without the t^2 gain recovery, and only the water layers are clearly visible. When the t^2 gain recovery is applied (Fig. 11b), two clear "water reflectors" show up at 8 and 13.5 ms. Particularly remarkable is the strip of 1 ms just above the seafloor, which is totally saturated from about 19 ms on. As 1 ms two-way traveltime, with a sea water velocity of 1500 m/s, corresponds to 75 cm, this strip may correspond to benthonic algae or very loose mud with a thickness of around 75 cm. Similar features are found also in other profiles where the seafloor is a bit shallower, as in the line G05-C02 in Fig. 12. Here a major plume is visible close to the shot point 22400, and clear water reflectors are visible at 8, 11, and 14 ms.

The reflectivity at the boundaries of sea-water layers is mainly due to sharp changes in temperature, as the P-wave velocity in the sea water depends mainly on it and, at a smaller extent, on salinity and depth (Rajan and Frisk, 1992; Terrill and Melville, 1997; Zou *et al*., 2015). Terrill and

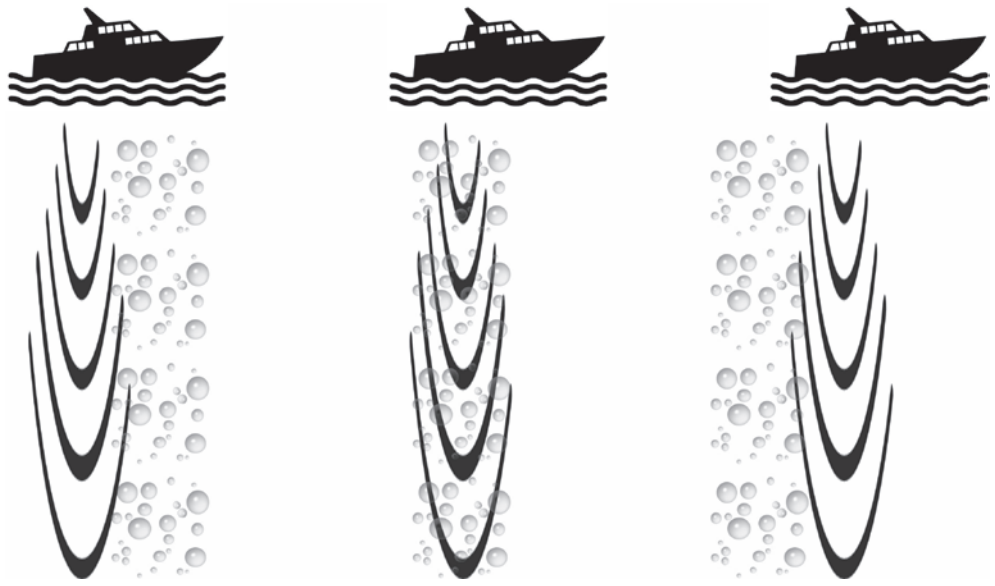

Fig. 10 - Possible effect of plumes to the Chirp survey. The bubbly zone may overlap partly (sides) or completely (centre) with the area covered by the radiation pattern of the Chirp source, during the ship navigation across the plume area.

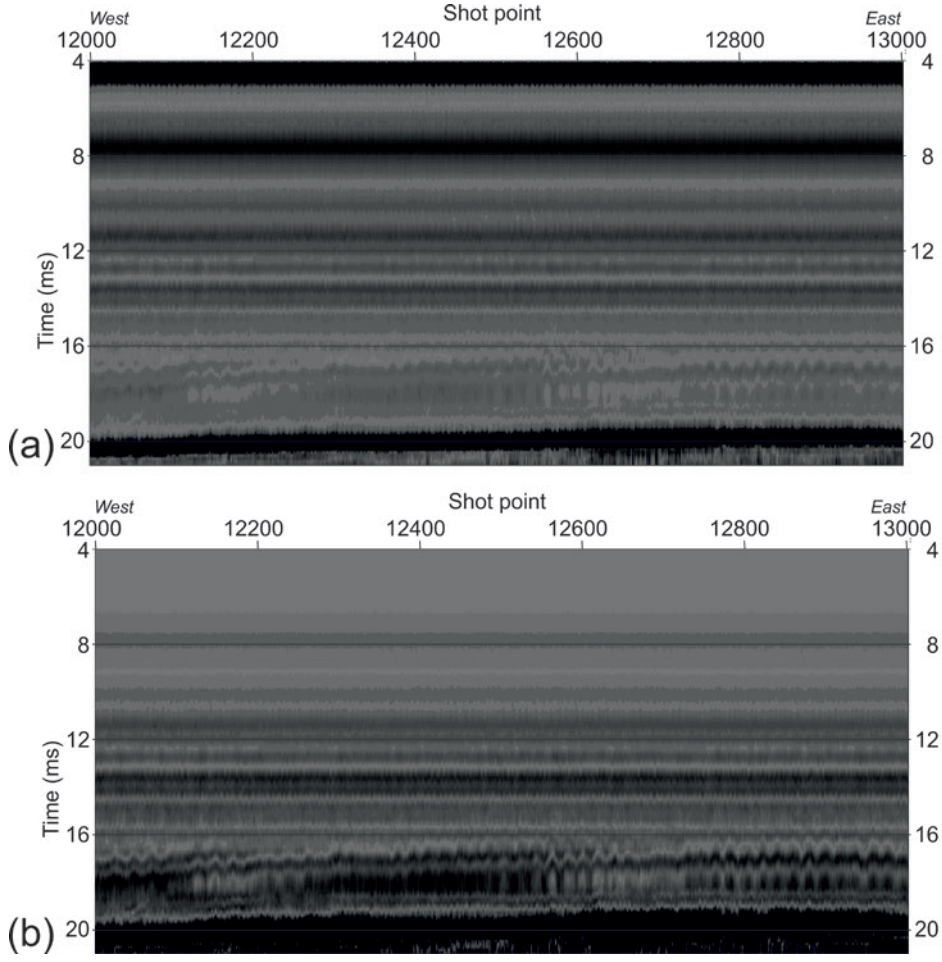

Fig. 11 - Vertically exaggerated detail in the profile G05-C02 with the traces between the sea surface and floor, using a global normalisation only (a) and after t^2 gain recovery (b).

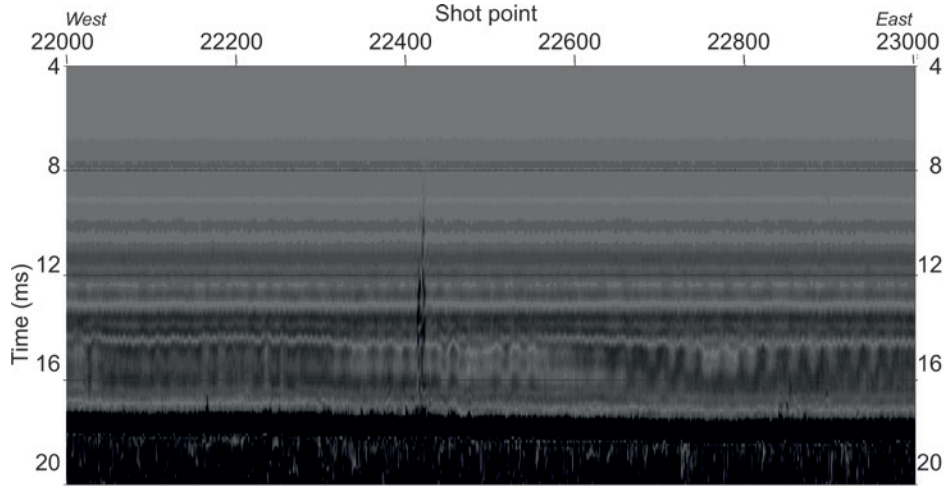

Fig. 12 - Vertically exaggerated detail of the traces between the sea surface and floor, after t^2 gain recovery, in the profile G05-C02. A plume in the water column is clearly imaged close to the shot point 22400.

Melville (2000) measured the effect of air bubbles to both P-wave velocity and sound absorption in the sea water. The use of seismic surveys to detect even complex and deep sea-water boundaries has been validated experimentally by Petronio *et al.* (2009, 2010), among others. Of course, temperature-related anomalies depend on seasons and weather conditions (see e.g. Cardin and Celio, 1997; Malačič *et al.,* 2006), so we may expect different water layering when repeating these surveys over time. This type of analysis may be critical for time-lapse seismic surveys (see e.g. Vesnaver *et al*., 2003).

The imaging of the plume within the water column by wiggle traces shows clearly their scattering along the traces, rising from the seafloor up to 5 ms below the sea surface. As the plume affects few adjacent traces, it can be appreciated only by considerably expanding the lateral scale. For this reason they cannot be visible at a very compressed lateral scale, as in Fig. 2.

Figs. 13, 14, and 15 show parts of the profile GT09-C21 where plumes from the seafloor are clearly evident, because the anomalies starting from the seafloor are not involving a single trace, but many, with a clear spatial pattern. In the lower part, we notice that under the plumes there are blanked zones, due to gas saturation. To highlight the plumes, in the upper part, we had to

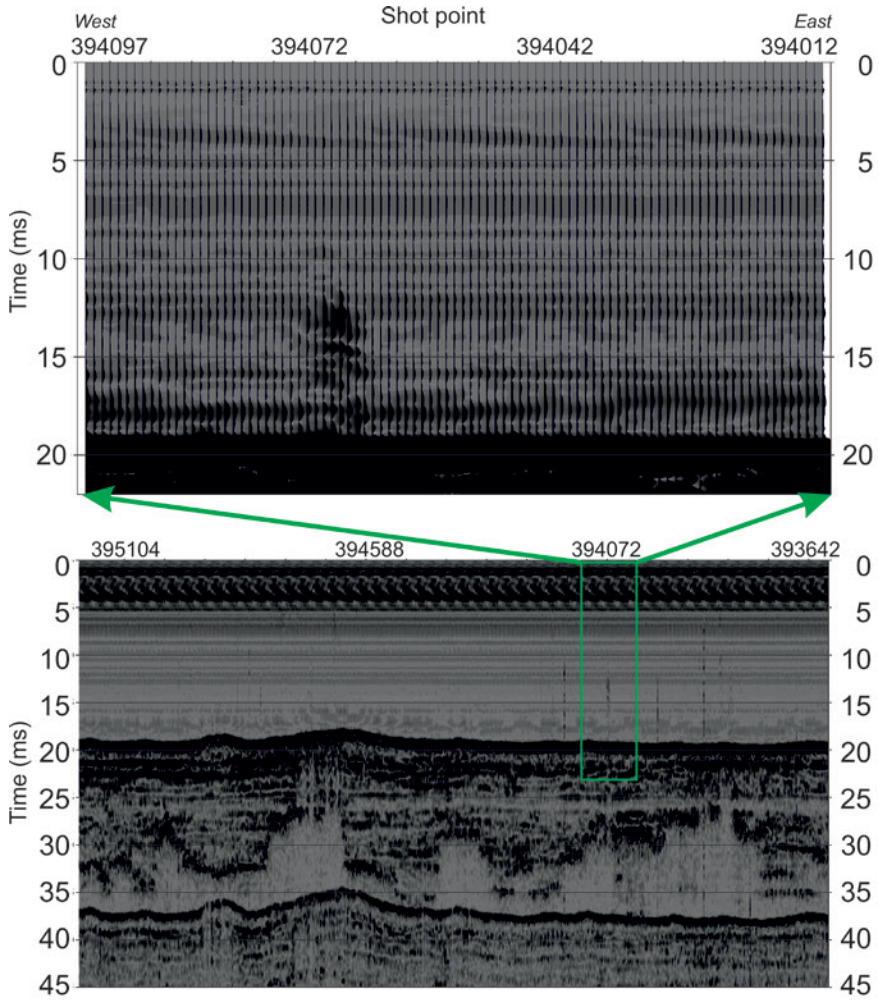

Fig. 13 - Partial section of the line GT09-C21 (upper part, raw data) and enlarged detail including an interpreted plume in the sea water (lower part, after a t^2 gain curve). The "vertical bars" in the lower section are more evident before the gain curve application, while the opposite happens for the plume emitted at the seafloor (upper section).

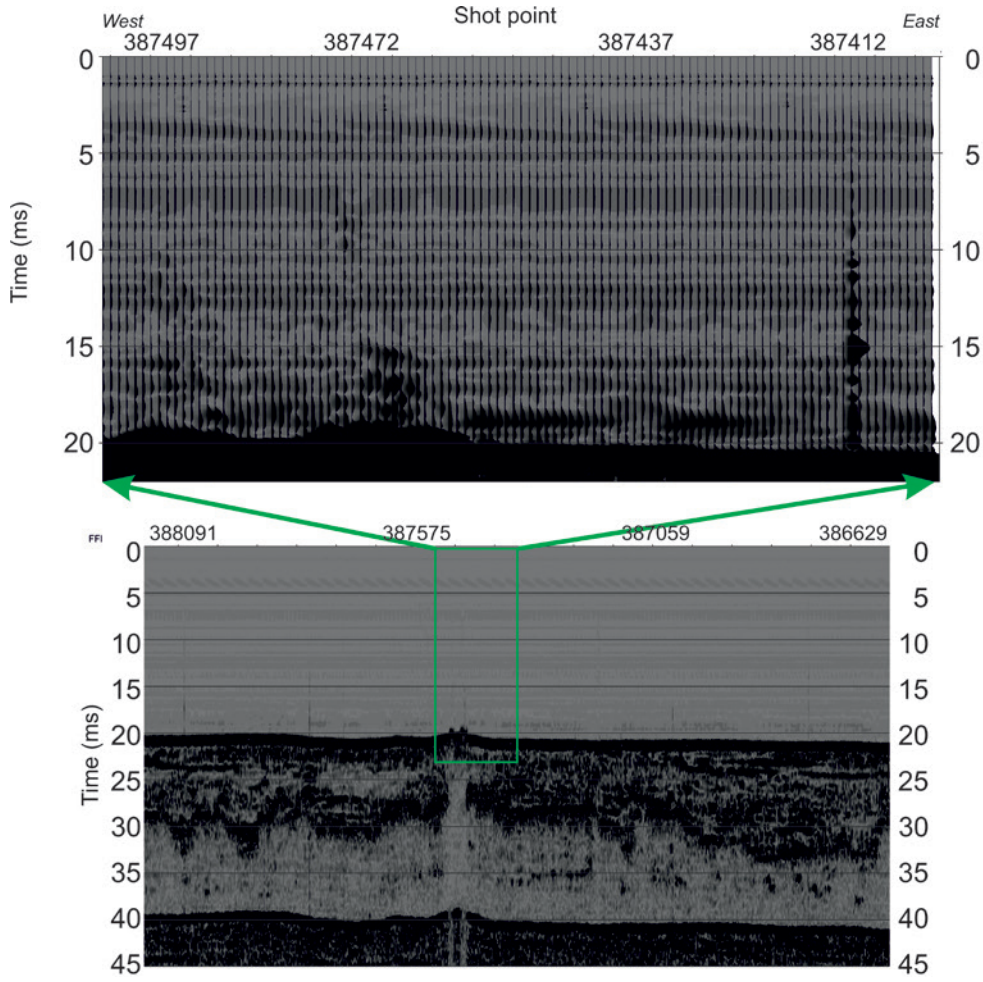

Fig. 14 - Partial section of the line GT09-C21 (lower part) and enlarged detail including an interpreted plume in the sea water (lower part) after a t^2 gain curve. The relieves at the seafloor are the "trezze".

boost significantly the signal, because the plume reflectivity is very low. However, note that in the lower part of Fig. 13 we did not apply the t^2 gain curve (unlike in Figs. 14 and 15) because in this way the "vertical bars" mentioned earlier are better visible, on both sides of the green rectangle. This shows the co-occurrence of the two phenomena (actual plumes and possible vertical "bubbles"), which are highlighted using different gain recovery types.

4. Geological interpretation

The Gulf of Trieste is characterised by a few metre-thick Holocene marine sediment, mainly silty clay (Covelli *et al.*, 2006), that in the Chirp profile are imaged by a transparent homogeneous acoustic facies. This unit covers the complex morphologies of the Late Pleistocene continental-paralic sediment (Trobec *et al.*, 2018, and references therein) that exhibits locally geometries of channel levee systems, typical of a fluvial plain environment. The Late Pleistocene continental-

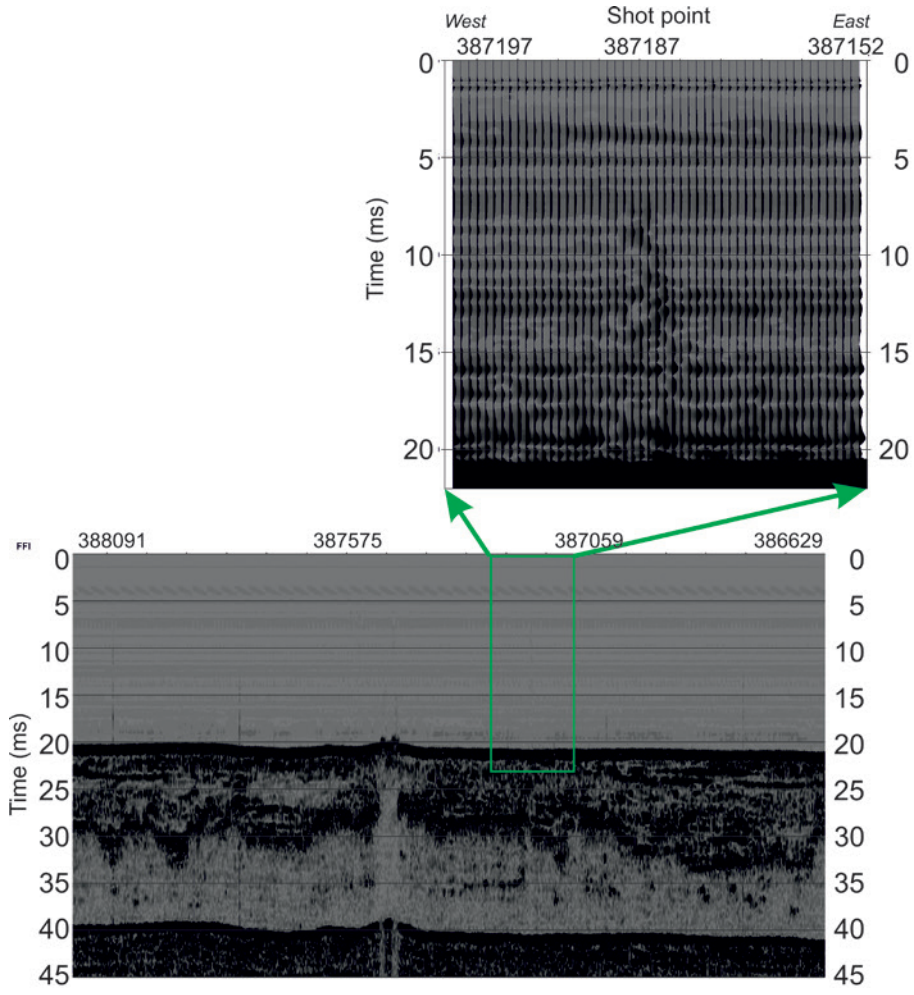

Fig. 15 - Partial section of the line GT09-C21 (lower part) and enlarged detail including an interpreted plume in the sea water (lower part) after a t^2 gain curve. The relieves at the seafloor are the "trezze".

paralic unit is some tens metre-thick, and overlies the Late Pleistocene marine sediment, with sub-horizontal stratification (Fig. 2). In addition to the stratigraphic geometries, the Chirp data show peculiar high-amplitude events with saw-tooth geometries, which are the top of the acoustic transparent facies. This facies has been interpreted to be fluid bearing sediment (Busetti *et al.*, 2020).

The applied processing enhances the imaging of the data, highlighting high-amplitude events with saw-tooth geometries, in particular those present in Figs. 8 and 9 around shot points 350000, below a channel levee system. These features are characterised by an acoustic transparent facies due to the scattering of poorly sorted sediment, typical of this sedimentary unit, which weakens the underlying reflections.

Both the t^2 gain and the gapped deconvolution (Fig. 8) improve the imaging of the deeper stratigraphic events. The multiple subtraction (Fig. 9a) improves the imaging of the high amplitude events almost coincident with the seafloor multiple.

In Fig. 9b, the combination of the different techniques, previously applied separately, as the

FX deconvolution using a lateral window of 3 traces only, after a t^2 gain curve and a gapped deconvolution, enhances the sharpness of the deeper stratigraphy, and allows distinguishing better stratigraphic horizons from high-amplitude reflectors at the top of the gas-bearing sediment. A better evidence of high-amplitude reflector is obtained also in the western side of Fig. 9b, which in the raw data of Fig. 2c are not so evident.

In the eastern part of the gulf (Fig. 2c and Figs. 8 and 9), the high-amplitude reflectors lie preferentially at ~50 ms, ~55 ms, ~59 ms, within the Late Pleistocene marine unit. In the western part of the gulf (Fig. 2b), the high-amplitude reflectors are shallower, from 30 to 45 ms, a few metres below the seafloor, providing fluid seeps (Fig. 2b and Figs. 12 to 15).

5. Discussion

The large toolbox of seismic processing that is available for standard surveys is much more limited when it comes to Chirp data, recording normally only the envelope of the signal. The phase information loss prevents using sophisticated and effective algorithms for multiple reflections' attenuation based on the wave equation. In our data set, another piece of information was lost during the acquisition by recording the signal by integer numbers (i.e. 16 bit), instead of floating point (32 bit). The advantage of that choice is halving the data size, which still remains relevant, but with a limited dynamic range. The latter drawback is one of the reasons for the limited success of the gapped deconvolution, which was able to remove visually the multiples, but unable to reveal the possible underlying weaker signals. We expect that a better recording of the signal by full digit precision and the actual waveform (i.e. without taking the envelope) could produce also in this area the excellent results presented by Baradello (2014) for a much more complex area.

Based on the available data, we can hypothesise that the "vertical bars" visible in the sections may be due to plumes of fluids emanating from the seafloor. This hypothesis is geologically reasonable, but additional measurements by independent methods are needed to validate this idea. Instead, the water layers due to near-vertical variations of temperature, salinity and probably also suspended particles are very reliable, as observed and validated elsewhere even using seismic sources with a lower resolution than Chirp. This success suggests further work as 3D imaging and monitoring over time of the sea-water masses.

6. Conclusions

The application of the Hilbert transform during acquisition provides "easy to use" data that may be interpreted without further processing, but prevents many more sophisticated processing techniques. Nevertheless, some processing tools can still be applied to the Hilbert-transformed wavelet to improve the imaging of the acoustic facies. The simple workflow of a t^2 gain recovery followed by a gapped deconvolution provides satisfying results in terms of interpretability of Chirp data. We cannot claim that the multiple subtraction provides better results in general, but in our case the first water-bottom multiple was better attenuated. Furthermore, a t^2 gain recovery is effective in revealing the water layers without the heavy distortions introduced by AGC. This part of the data, normally ignored, contains precious information for oceanographic studies and environment protection. We imaged several plumes associated to ongoing fluids' release from the seafloor. The techniques presented provide new perspectives in using single-channel high-

resolution data for a better stratigraphic and fluid occurrences definition. They validated the presence of plumes in the water column by the co-occurrence of independent elements at the same point, such as the blanking zones due to fluid accumulation and the “trezze”. The use of these studies might be the control of coastal erosion, engineering of offshore infrastructures and general climate studies.

REFERENCES

Baeten G. and Ziolkowski A.; 1990: *The Vibroseis source*. Elsevier, Amsterdam, The Netherlands, 299 pp.

Baradello L.; 2014: *An improved processing sequence for uncorrelated Chirp sonar data*. Mar. Geophys. Res., 35, 337-344.

Busetti M., Volpi V., Nicolich R., Barison E., Romeo R., Baradello L., Brancatelli G., Giustiniani M., Marchi M., Zanolla C., Wardell N., Nieto D. and Ramella R.; 2010: *Dinaric tectonic features in the Gulf of Trieste (northern Adriatic)*. Boll. Geof. Teor. Appl., 51, 117-128.

Busetti M., Zgur F., Vrabec M., Facchin L., Pelos C., Romeo R., Sormani L., Slavec P., Tomini I., Visnovic G. and Zerial A.; 2013: *Neotectonic reactivation of Meso-Cenozoic structures in the Gulf of Trieste and its relationship with fluid seepings*. In: Proc. 32nd Convegno del Gruppo Nazionale di Geofisica della Terra Solida (GNGTS), Trieste, Italy, pp. 29-34.

Busetti M., Babich A. and Del Ben A.; 2020: *Evidenze geofisiche di emissioni di fluidi nel Golfo di Trieste (nord Adriatico*). In: D’Angelo S., Battaglini L. and Fiorentino A. (eds), Inventario delle emissioni fluide nei mari italiani, Memorie Descrittive della Carta Geologica d’Italia, D.R.E.Am, Firenze, Italy, Vol. 105, pp. 11-16.

Canales L.L.; 1984: *Random noise reduction*. In: Expanded Abstracts, 54th SEG Annual Meeting, Atlanta, GA, USA, pp. 525-527, doi: 10.1190/1.1894168.

Cardin V. and Celio M.; 1997: *Cluster analysis as a statistical method for identification of the water bodies present in the Gulf of Trieste (northern Adriatic Sea)*. Boll. Geof. Teor. Appl., 38, 119-135.

Casero P.; 2004: *Structural setting of petroleum exploration plays in Italy*. In: Crescenti U., D’Offizi S., Merlino S. and Sacchi L. (eds), 32nd International Geological Congress, Italian Geological Society, Firenze, Italy, Special Volume, pp. 189-199.

Cassano E. and Rocca F.; 1973: *Multichannel linear filters for optimal rejection of multiple reflections*. Geophys., 38, 1053-1061.

Conti A., Stefanon A. and Zuppi G.M.; 2002: *Gas seeps and rock formation in the northern Adriatic Sea*. Cont. Shelf Res., 22, 2333-2344.

Covelli S., Fontolan G., Faganeli J. and Ogrinc N.; 2006: *Anthropogenic markers in the Holocene stratigraphic sequence of the Gulf of Trieste (northern Adriatic Sea)*. Mar. Geol., 230, 29-51, doi: 10.1016/j.margeo.2006.03.013.

Duarte H., Menezes Pinheiro L., Curado Teixeira F. and Monteiro J.H.; 2007: *High-resolution seismic imaging of gas accumulations and seepage in the sediments of the Ria de Aveiro barrier lagoon (Portugal).* Geo-Mar. Lett., 27, 115-126, doi: 10.1007/s00367-007-0069-z.

Ehrenberg J. and Torkelson T.; 2000: *FM slide (Chirp) signals: a technique for significantly improving the signal-to-noise performance in hydroacoustic assessment systems*. Fish. Res., 476, 193-199, doi: 10.1016/S0165-7836(00)00169-7.

EMODnet Bathymetry Consortium; 2018: *EMODnet digital bathymetry (DTM 2018)*. <https://www.emodnet.eu>.

Foster D.J. and Mosher C.C.; 1992: *Suppression of multiple reflections using the Radon transform*. Geophys., 57, 386-395.

Fowler P. and Claerbout J.F.; 1983: *An estimator of seismic amplitude decay*. Stanford Explor. Project, 38, 73-88.

García-Gil S., Vilas F. and García-García A.; 2002: *Shallow gas features in incised-valley fills (Ria de Vigo, NW Spain): a case study*. Cont. Shelf Res., 22, 2303-2315, doi: 10.1016/S0278-4343(02)00057-2.

Gordini E., Caressa S. and Marocco R.; 2003: *New morpho-sedimentological map of the Trieste Gulf (from Punta Tagliamento to Isonzo Mouth).* Atti del Museo Friulano di Storia Naturale, 35, 5-29.

Gordini E., Marocco R., Tunis G. and Ramella R.; 2004: *I depositi cementati del Golfo di Trieste (Adriatico Settentrionale): distribuzione areale, caratteri geomorfologici e indagini acustiche ad alta risoluzione.* Il Quaternario, 17, 555-563.

Gordini E., Falace A., Kaleb S., Donda F., Marocco R. and Tunis G.; 2012: *Methane-related carbonate cementation of marine sediments and related macroalgal coralligenous assemblages in the northern Adriatic Sea*. In: Harris P.T. and Baker E.K. (eds), Sea floor geomorphology as benthic habitats, Elsevier, Amsterdam, The Netherlands, pp. 183-198.

Gulunay N.; 1986: *FXDECON and complex Wiener prediction filter*. In: Expanded Abstracts, 56th SEG Annual Meeting, Houston, TX, USA, pp. 279-281.

Gulunay N.; 2017: *Signal leakage in f-x deconvolution algorithms*. Geophys., 82, W31-W45.

Henkart P.; 2006: *Chirp sub-bottom profiler processing - a review*. Sea Technol., 47, 35-38.

Hovland M. and Curzi P.; 1989: *Gas seepage and assumed mud diapirism in the Italian central Adriatic Sea*. Mar. Petrol. Geol., 6, 161-169.

Kelamis P.G. and Mitchell A.R.; 1989: *Slant-stack processing*. First Break, 7, 43-54.

Kim G.Y., Kim D.C., Park S.C. and Lee G.H.; 1999: *Chirp (2-7 kHz) echo characters and geotechnical properties of surface sediments in the Ulleung Basin, the East Sea*. Geosci. J., 3, 213-224.

Malačič V., Celio M., Čermelj B., Bussani A. and Comici C.; 2006: *Interannual evolution of seasonal thermohaline properties in the Gulf of Trieste (northern Adriatic) 1991-2003*. J. Geophys. Res., 111, C08009, doi: 10.1029/2005JC003267.

Morgante S.; 1940: *I "bromboli" delle coste istriane*. Notiziario dell'Istituto di Biologia Rovigno, 16/2, 1-12.

Petronio L., Lipizer M., De Santis L., Rintoul S. and Wardell N.; 2009: *Seismic reflections within the sea water column in the southern Ocean, Antarctica*. In: Proc. 71st EAGE Conference and Exibition, Amsterdam, The Netherlands, cp-127-00330, pp. 2312-2316, doi: 10.3997/2214-4609.201400337.

Petronio L., Lipizer M., De Santis L., Rintoul S. and Wardell N.; 2010: *Offshore seismic reflection data: an oceanographic perspective*. Boll. Geof. Teor. Appl., 51, 89-98.

Pham L.D. and Lau A.; 1997: *Optimal multiple extrapolation and attenuation*. In: Expanded Abstracts, 67th SEG Annual Meeting, Dallas, TX, USA, pp. 1173-1175.

Quinn R., Bull J.M. and Dix J.K.; 1998: *Optimal processing of marine high-resolution seismic reflection (Chirp) data*. Mar. Geophys. Res., 20, 13-20.

Rajan S.D. and Frisk G.V.; 1992: *Seasonal variations of the sediment compressional wave-speed pro-file in the Gulf of Mexico*. J. Acoust. Soc. Am., 91, 127-135.

Robinson E.A.; 1967: *Predictive decomposition of time series with applications to seismic exploration*. Geophys., 32, 411-484, doi: 10.1190/1.1439873.

Robinson E.A.; 1983: *Multichannel time series analysis with digital computer programs. 2nd ed.* Goose Pond Press, Houston, TX, USA, 455 pp.

Robinson E. and Treitel S.; 1980: *Geophysical signal analysis*. Prentice-Hall, Englewood Cliffs, NJ, U.S.A., 466 pp.

Taner M.T.; 1980: *Long-period sea-floor multiples and their attenuation*. Geophys. Prospect., 28, 30-48.

Terrill E.J. and Melville W.K.; 1997: *Sound-speed measurements in the surface-wave layer.* J. Acoust. Soc. Am., 102, 2607, doi: 10.1121/1.420315.

Terrill E.J. and Melville W.K.; 2000: *A broadband acoustic technique for measuring bubble size distributions: laboratory and shallow water measurements.* J. Atmos. Oceanic Technol., 17, 220-239.

Tóth Z., Spiess V. and Jensen J.B.; 2014: *Seismo-acoustic signatures of shallow free gas in the Bornholm Basin, Baltic Sea.* Cont. Shelf Res., 88, 228-239.

Trobec A., Busetti M., Zgur F., Baradello L., Babich A., Cova A., Gordini E., Romeo R., Tomini I., Poglajen S., Diviacco P. and Vrabec M.; 2018: *Thickness of marine Holocene sediment in the Gulf of Trieste (northern Adriatic Sea)*. Earth Syst. Sci. Data, 10, 1077-1092, doi: 10.5194/essd-10-1077-2018.

Verschuur D.J., Berkhout D.J. and Wapenaar C.P.A.; 1992: *Adaptive surface-related multiple elimination*. Geophys., 57, 1166-1177.

Vesnaver A., Accaino F., Böhm G., Madrussani G., Pajchel J., Rossi G. and Dal Moro G.; 2003: *Time-lapse tomography*. Geophys., 68, 815-823.

Vesnaver A., Böhm G., Cance P., Carcione J.M. and Gei D.; 2020: *Windowless Q-factor tomography by the instantaneous frequency*. Geophys. Prospect., 68, 2611-2636.

Wiggins J.W.; 1988: *Attenuation of complex water-bottom multiples by wave-equation-based prediction and subtraction*. Geophys., 53, 1527-1539.

Yilmaz Ö.; 2001: *Seismic data analysis. Processing, inversion, and interpretation of seismic data - Volume I, 2nd ed*. Society of Exploration Geophysicists, Tulsa, OK, USA, 2041 pp., doi: 10.1190/1.9781560801580.

Zampa L.S.; 2020: *New bathymetric maps of the north east Adriatic Sea*. Istituto Nazionale di Oceanografia e di Geofisica Sperimentale - OGS, Trieste, Italy, Technical Report 05/2020OGS, 11 pp.

Zou D., Williams K.L. and Thorsos E.I.; 2015: *Influence of temperature on acoustic sound speed and attenuation of sea floor sand sediment*. IEEE J. Oceanic Eng., 40, 969-980.

Corresponding author: Aldo Vesnaver
Istituto Nazionale di Oceanografia e di Geofisica Sperimentale - OGS
Borgo Grotta Gigante 42c, 34010 Sgonico (TS), Italy
Phone: +39 040 21401; e-mail: avesnaver@inogs.it

Appendix

The complex trace $c(t)$ related to the recorded trace $s(t)$ is defined as:

$$c(t) = s(t)) + \mathrm{i}\, \mathrm{H}\{s(t)\} = s(t) + \mathrm{i}\, s'(t) \quad \text{(A-1)}$$

where the prime is an abbreviation for the Hilbert transform operator and i indicates the imaginary unit. Using Eq. 2, we get:

$$c(t) = r(t) * [w(t) + \mathrm{i}\, w'(t)]. \quad \text{(A-2)}$$

The envelope $e(t)$ is the module of the complex trace:

$$e(t) = |c(t)| = [c(t)\, c^*(t)]^{1/2}, \quad \text{(A-3)}$$

where $c^*(t)$ is the complex conjugate of $c(t)$. Multiplying Eq. A-2 by its complex conjugate, we get:

$$c(t)\, c^*(t) = \{r(t) * [w(t) + \mathrm{i}\, w'(t)]\}\, \{r(t) * [w(t) - \mathrm{i}\, w'(t)]\}, \quad \text{(A-4)}$$

as the reflectivity $r(t)$ is a real function, and thus: $r^*(t) = r(t)$. Rearranging Eq. A-4, we obtain:

$$c(t)\, c^*(t) = r^2(t) * [w^2(t) + w'^2(t)], \quad \text{(A-5)}$$

and substituting Eq. A-5 into Eq. A-3, we get finally:

$$e(t) = |r(t)| * [w^2(t) + w'^2(t)]^{1/2}. \quad \text{(A-6)}$$

This expression highlights the loss of the polarity information in the envelope $e(t)$: we can only retrieve the reflectivity module $|r(t)|$ from it, even if we know perfectly the wavelet $w(t)$.

Fig. A-1 is a simple example of a 1D reverberation between the sea surface and seafloor. The values assumed for the air, sea water and shallow sediments are 330, 1500, and 2000 m/s for the P velocity, and 1.225, 1029 and 2000 kg/m^3 for the density. As a result, the reflection coefficients for the air/water and water/sediments are 0.999 and 0.443, respectively. These values may approximate those ones of the Chirp surveys we are studying. Trace 1 shows the reflectivity of the seafloor primary and all the following reverberations. Trace 2 is the convolution of a minimum-phase wavelet obtained by a Butterworth filter with a frequency range from 10 to 80 Hz. Trace 3 is its envelope. Taking the gapped deconvolution of traces 2 and 3, we get the deconvolved traces 4 and 5, respectively. The operator gap was 70 ms, and the total length was 170 ms. These values were chosen because the seafloor reflection occurs at 80 ms. The reverberations removal is excellent, both for the standard trace (4) and its envelope (5).

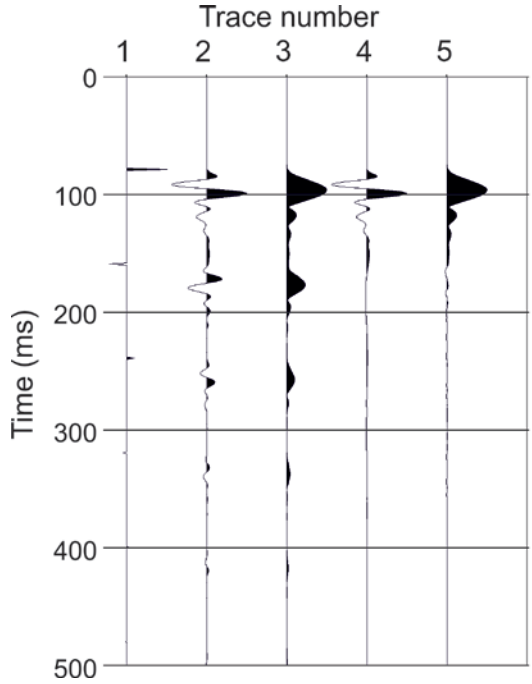

Fig. A-1 - Deconvolution test: trace 1 = spikes for a reverberation; trace 2 = convolution with a wavelet; trace 3 = envelope of trace 2; trace 4 = deconvolution of trace 2; trace 5 = deconvolution of trace 3, which is identical to the envelope of trace 4.